chemosensors

MDPI

Article

Self-Assembly of Ultrathin Nickel Oxysulfide for Reversible Gas Sensing at Room Temperature

Nam Ha [1], Kai Xu [1,*], Yinfen Cheng [2], Rui Ou [1], Qijie Ma [1], Yihong Hu [1], Vien Trinh [1], Guanghui Ren [1], Hao Yu [2], Lei Zhang [3,4], Xiang Liu [3,4], Jiaru Zhang [1], Zhong Li [2] and Jian Zhen Ou [1,2,*]

[1] School of Engineering, RMIT University, Melbourne, VIC 3000, Australia
[2] Key Laboratory of Advanced Technologies of Materials, Ministry of Education, School of Materials Science and Engineering, Southwest Jiaotong University, Chengdu 610031, China
[3] College of Civil Aviation Safety Engineering, Civil Aviation Flight University of China, Deyang 618307, China
[4] Civil Aircraft Fire Science and Safety Engineering Key Laboratory of Sichuan Province, Deyang 618307, China
* Correspondence: kai.xu@rmit.edu.au (K.X.); jianzhen.ou@rmit.edu.au (J.Z.O.)

Abstract: Two-dimensional (2D) or ultrathin metal sulfides have been emerging candidates in developing high-performance gas sensors given their physisorption-dominated interaction with target gas molecules. Their oxysulfide derivatives, as intermediates between oxides and sulfides, were recently demonstrated to have fully reversible responses at room temperature and long-term device stability. In this work, we explored the micro-scale self-assembly of ultrathin nickel oxysulfide through the calcination of nickel sulfide in a controllable air environment. The thermal treatment resulted in the replacement of most S atoms in the Ni-S frameworks by O atoms, leading to the crystal phase transition from original hexagonal to orthorhombic coordination. In addition, the corresponding bandgap was slightly expanded by ~0.15 eV compared to that of pure nickel sulfide. Nickel oxysulfide exhibited a fully reversible response towards H_2 at room temperature for concentrations ranging from 0.25% and 1%, without the implementation of external stimuli such as light excitation and voltage biasing. The maximum response factor of ~3.24% was obtained at 1% H_2, which is at least one order larger than those of common industrial gases including CH_4, CO_2, and NO_2. Such an impressive response was also highly stable for at least four consecutive cycles. This work further demonstrates the great potential of metal oxysulfides in room-temperature gas sensing.

Keywords: nickel oxysulfide; room temperature gas sensing; H_2 sensor; physisorption

Citation: Ha, N.; Xu, K.; Cheng, Y.; Ou, R.; Ma, Q.; Hu, Y.; Trinh, V.; Ren, G.; Yu, H.; Zhang, L.; et al. Self-Assembly of Ultrathin Nickel Oxysulfide for Reversible Gas Sensing at Room Temperature. *Chemosensors* **2022**, *10*, 372. https://doi.org/10.3390/chemosensors10090372

Academic Editor: Simonetta Capone

Received: 19 July 2022
Accepted: 15 September 2022
Published: 17 September 2022

1. Introduction

Two-dimensional (2D) materials, consisting of single or few atomic layers, have been considered as emerging candidates for high-performance gas sensing featured with excellent sensitivity, high selectivity, and low power consumption [1–6]. Differing from the conventional chemisorption mechanism, the interaction of gas molecules with the surface of 2D materials most likely follows the model of physisorption without the involvement of adsorbed oxygen [1,3,6,7]. Particularly, the direct adsorption of gas molecules leads to the generation of electrical dipoles at the gas-matter interface in the presence of the charge transfer [1,3,7–9]. The concentration of surface adsorbed molecules is dependent on the surface adsorption energy of the 2D material, while the magnitude and direction of the charge transfer are correlated with the relative electronic band positions of the 2D material in reference to the molecule band positions of the gas [7–9]. As a result, the presence of interfacial electrical dipoles significantly re-distributes the charge carriers within the ultrathin 2D material body, leading to the observable variation of electrical resistance which can be used as the transduction output signal [1,3,7–9]. The early exploration of graphene and its derivatives demonstrates the feasibility of developing such physisorption-based gas sensors operated at room temperature [2,10–12]. However, their strong surface adsorption

energies cause the prolonged or failure desorption of targeted gas molecules in the recovery phase, making the sensor irreversible or with impractical recovery kinetics [10,13–15].

Investigations focused on layered 2D metal sulfides, particularly post-transition metal sulfide (e.g., SnS_2 and SnS), have shone a light onto the realization of reversible physisorption-based gas sensors [1,5,7,16–19]. For instance, 2D few-layered SnS_2 exhibits reversible NO_2 gas sensing at the optimum temperature of 120 °C with minimum cross-talk from humidity and high selectivity of NO_2 over other commonly-seen industrial gases (e.g., H_2, H_2S, CO_2, and CH_4), while the limit of detection (LOD) is estimated at ~30 ppb [1]. Furthermore, the implementation of 2D few-layered SnS lowers the operating temperature down to 60 °C with the assistance of broadband visible light excitation [5]. The sensitivity of NO_2 detection is maintained and the LOD is further reduced to 8 ppb. Inspired by the above-mentioned results, recent studies have also been extended to non-layered ultra-thin metal sulfides. For example, ultra-thin In_2S_3 nanoflakes doped with N elements are self-assembled into three-dimensional (3D) micro-combs, exhibiting reversible NO_2 sensing performances at room temperature with a small LOD of ~2.2 ppb [9].

Nevertheless, most 2D metal sulfides are inherently sensitive to oxygen, being easily transformed into metal oxysulfides or sulfates as intermediates of the oxidation reaction [3,6,20]. To induce full conversion, power-intensive approaches (e.g., calcination [20] and probe-sonication [3,6]) need to be applied, in which part of the sulfide atoms is replaced by oxygen atoms within the metal-sulfide framework. Interestingly, this group of materials has been recently brought to attention for their strong potential in gas sensing owing to the modified electronic band structures and improved long-term stabilities in comparison with those of the metal sulfide counterparts, while the physisorption remains the dominant gas adsorption model. Ultra-thin Janus indium oxysulfide (InS_xO_y)/In_2S_3 within the category of post-transition metal was realized using a power-intensive probe-sonication approach, exhibiting a visible-light-driven reversible, room temperature, and selective NO_2 optoelectronic gas-sensing performance with an extremely low LOD of 0.363 ppb [3]. In addition, a similar synthesis method was applied to palladium sulfide (PdS) as a representative in the category of noble metal, leading to the formation of 2D palladium oxysulfide with the reversible NO_2 sensing response occurring at room temperature without the implementation of light excitation [6]. Although the metal oxysulfides have been increasingly realized in gas sensors, the application of the material group for H_2 detection is still in an early stage [21].

In this work, we explore the category of ultra-thin transition metal oxysulfide for the investigation of room temperature reversible gas sensing, in which nickel oxysulfide is selected as the representative. The deposition of ultra-thin planar materials onto the sensor substrate conventionally leads to the formation of the compact surface assembled in a layer-by-layer manner, which may limit the exposure surface area with the gas molecules as well as the gas adsorption/desorption kinetics. Instead, we obtain nickel oxysulfide in the form of 3D hierarchical micro-flowers self-assembled from ultra-thin 2D nanoflakes, which is achieved through the direct calcination approach of 3D nickel sulfide (NiS) in a controlled environment [20,22,23]. Subsequently, the morphology, crystal structure, chemical composition, and band structure of nickel oxysulfide are revealed. The room temperature gas sensing performances are investigated, in which the reductive H_2 gas is selected as the target instead of the oxidizing NO_2 gas (i.e., the most common gas investigated for 2D metal sulfides). A comparative study is also carried out against other commonly-seen oxidating and reducing gases such as CH_4, NO_2, and CO_2 [24].

2. Materials and Methods

2.1. Material Synthesis and Preparation

First, 237 mg of nickel chloride hexahydrate ($Cl_2H_{12}NiO_6$) (>99.0%) was mixed with 150 mg of thiourea (CH_4N_2S) (>99.0%), stirring with 40 mL of deionized (DI) water at 30 °C for 30 min at the speed of 500 revolutions per minute (rpm). After autoclaving at 150 °C for 25 h and following by cooling down to room temperature, the solution mixture was

centrifuged at 5000 rpm for 20 min to collect the precipitate. By dispersing the obtained sediment into DI water for another 20 min of centrifugal washing (5000 rpm), the nickel sulfide powder was prepared by drying the final obtained precipitate at 50 °C for 24 h. The prepared nickel sulfide powder was further annealed at 600 °C for 6 h at a ramping up speed of 300 °C h^{-1} with a constant flow rate of 200 standard cubic centimeters per minute (sccm) compressed dry air. Following a slow cool-down phase (at a ramping down speed of 300 °C per hour), the nickel oxysulfide was prepared by dispersing the annealed powder in 10 mL of ethanol solution.

2.2. Material Characterization

The micro-flower structure of nickel sulfide and nickel oxysulfide were investigated using a FEI Nova NanoSEM 200 (FEI Company, Hillsboro, OR, USA). JEOL JEM-F200 (Jeol, Tokyo, Japan) transmission electron microscopy with EDS detector (accelerating voltage of 200 kV) was carried out on nickel oxysulfide nanoflakes to examine the SAED pattern, crystal lattices, and chemical composition. XRD was characterized by a Bruker D4 ENDEAVOR (Bruker, Billerica, MA, USA) equipped with a monochromatic Cu Kα radiation source (λ = 0.154 nm). A Krato AXIS Supra XPS (Krato, Manchester, UK) with dual Al/Ag monochromatic X-ray source (Al Kα X-rays at 1486.7 eV) was used for XPS measurements. UV-Vis-NIR spectra were investigated using a Cary 500 spectrometer (Agilent, Santa Clara, CA, USA). Raman spectrum of nickel oxysulfide micro-flowers was collected by a HORIBA LabRAM HR Evolution (Horiba Scientific, Kyoto, Japan) with the excitation wavelength of 532 nm.

2.3. Sensor Fabrication and Measurements

An interdigital transducer (HORX Sensortech, Melbourne, Australia) including 200 pairs of gold electrodes in the spacing of 10 μm was utilized as the transducing substrate. Prior to drop-casting on the transducing substrate, the nickel oxysulfide sample solution prepared in 10 mL ethanol was sonicated for 10 min, which evenly disperses the material nanoflakes throughout the ethanol solution, before 20 μL of the nickel oxysulfide suspension was drop-casted onto the substrate as the H_2 sensor (Figure S1) [25]. Through a minimized probe stage built inside a customized gas chamber, the resistance of the sensor was monitored using an Agilent 34401A digital multimeter during the gas sensing experiments. Meanwhile, a computerized multichannel gas calibration system was applied to regulate an incoming gas stream at a constant flow rate of ~100 sccm entering the gas chamber from the inlet. The outlet of the gas chamber was connected to a back pressure regulator (Hy-Lok Oceania, Melbourne, Australia) to maintain the gas pressure of 1 standard atmosphere in the chamber.

3. Results and Discussion

3.1. Material Characterization

Pure nickel sulfide exhibits a micro-flower morphology according to the scanning electron microscope (SEM) image (Figure S2). After the calcination at 600 °C for 6 h with a constant airflow provided (details are presented in the Material Synthesis and Preparation section), the nickel sulfide converts to nickel oxysulfide with a hierarchical microstructure (sizes between 5 and 10 μm) as demonstrated by the SEM image in Figure 1a. From the low-resolution transition electron microscopy (TEM) image shown in Figure 1b, the nickel oxysulfide micro-flower structure is confirmed to be self-assembled from spherical nanoflakes with lateral dimensions of ~50 nm. Moreover, the thickness of those nanoflakes is known to be relatively small considering their highly transparent features (Figure 1b). The X-ray diffraction (XRD) measurements are carried out on both materials as shown in Figure 1c, in which the nickel oxysulfide presents a distinct crystal structure compared to that of the original pure NiS after a long-time oxygen annealing treatment. Sharp diffraction peaks are observed only at 38.1°, 43.8°, and 62.7°. Those peaks match well with the simulated crystal planes of (130), (221), and (151), respectively, based on the crystal

model of orthorhombic nickel sulfate (Figure S3) [26–28]. From the selected area electron diffraction (SAED) pattern and the corresponding high-resolution TEM (HRTEM) image for the nanoflakes shown in Figure 1d,e, the crystal planes of (130) and (151) are clearly identified with the lattice spacings of 0.24 and 0.15 nm directly measured from Figure 1e. In addition, an energy-dispersive X-ray spectroscopy (EDS) detector, integrated within TEM, is utilized to investigate the elemental composition of the nickel oxysulfide. According to Figure 1f, while Ni, O, and S are all found upon the nanoflakes, the significantly weaker S signals compared to those of O reveal that a dramatic replacement of sulfur by oxygen occurred during the calcination. Such a phenomenon is not observed in the nickel sulfide sample (Figure S4).

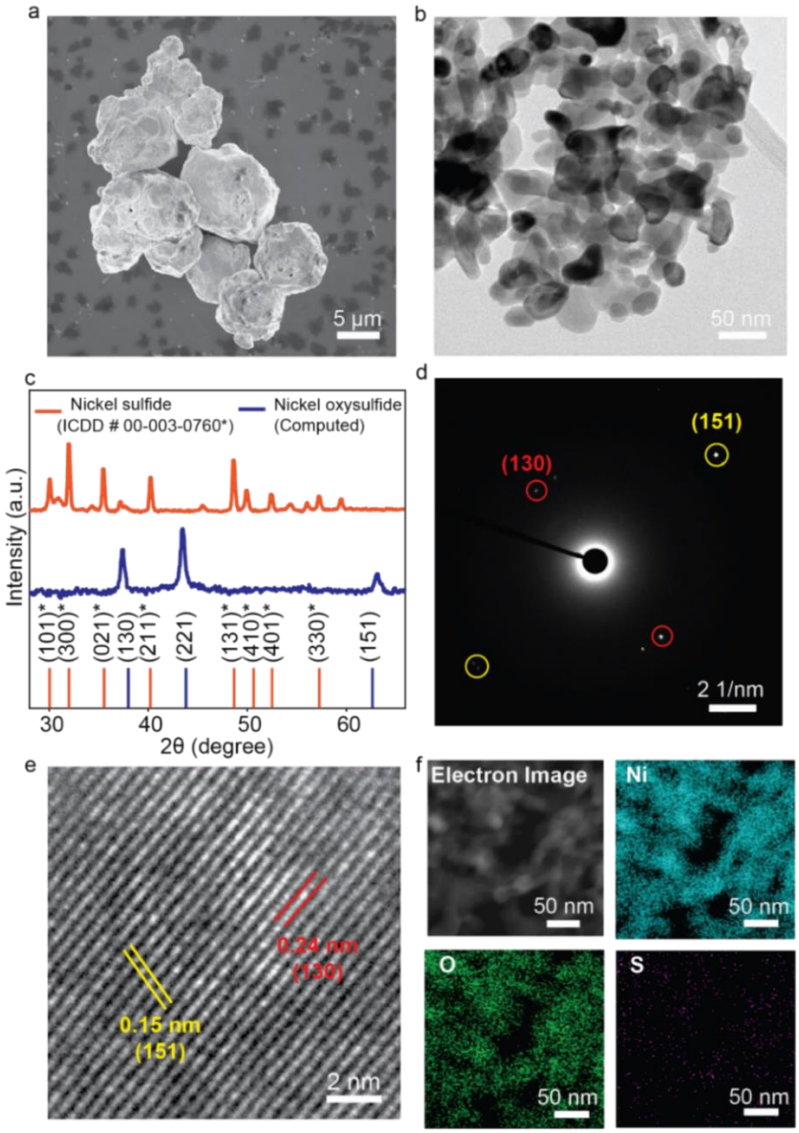

Figure 1. Material characterizations for nickel oxysulfide in (**a**) SEM, (**b**) TEM, (**c**) XRD measures for both nickel sulfide (indexed by ICDD # 00-003-0760; the corresponding crystal planes suffixed with '*') and nickel oxysulfide (the crystal planes simulated from $NiSO_4$ crystal model, space group Cmcm, a = 5.199 Å, b = 7.956 Å and c = 6.446 Å), (**d**) SAED, (**e**) HRTEM and (**f**) EDS analysis.

The overall chemical composition of the self-assembled nickel oxysulfide microflowers is assessed using X-ray photoelectron spectroscopy (XPS). From the Ni 2p spectrum shown in Figure 2a, a pair of small peaks located at ~853.31 and ~870.61 eV is considered as a doublet for Ni-S bond, while the main peak centered at ~854.98 eV together with its spin-orbit shoulder at ~872.28 eV can be assigned to the Ni-O bond [26,27,29–32]. Fur-

thermore, two typical satellite features, observed at ~860.74 and 878.42 eV, are consistent with the previous reports [26,27,29–33]. Figure 2b reveals a missing conventional S 2p peak of metal sulfide between 161 and 163 eV. Instead, a broad peak convoluted by an S3/2 (i.e., centered at 167.56 eV) and S1/2 (i.e., located at 168.72 eV) doublet is found at the S 2p spectrum, indicating the formation of S-O bonds as reports on metal oxysulfide materials have suggested [3,20,34,35]. From the O 1s spectrum shown in Figure 2c, the main peak sitting at 532.19 eV represents the existence of metal oxide, while the small hump in the region between 527 and 530 eV can be ascribed to the binding energy of the S-O bond [6,36].

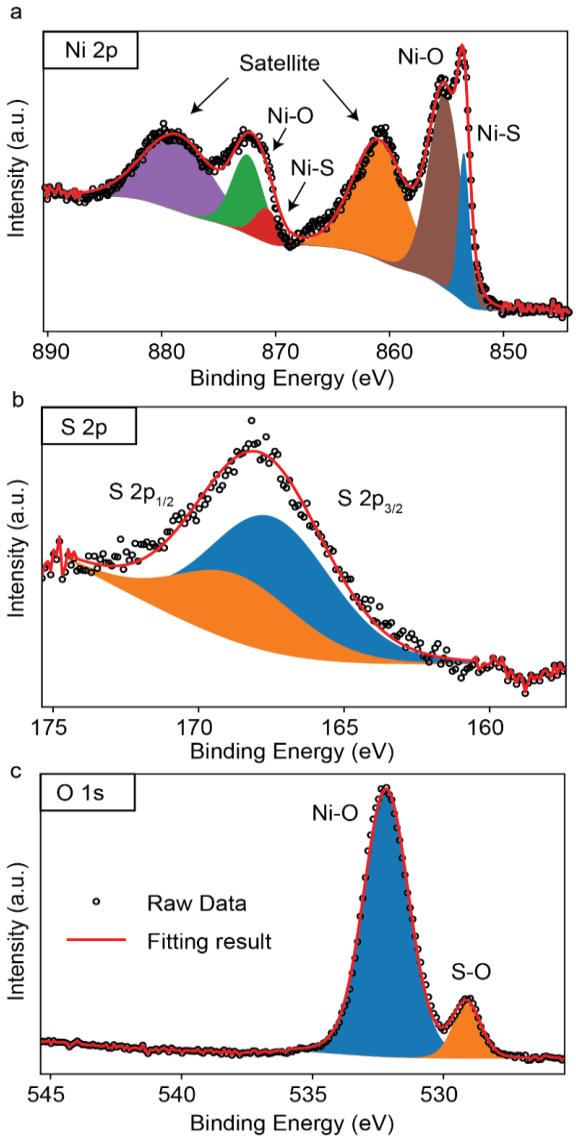

Figure 2. XPS measurement for nickel oxysulfide of (**a**) Ni 2p, (**b**) S 2p, and (**c**) O 1s spectrum.

The bonding information of the nickel oxysulfide is further confirmed using Raman spectroscopic measurements as shown in Figure 3a, in which relatively weak doublets found at 225 and 365 cm^{-1} are assigned to Ni-S bonding vibration [37,38]. In addition, strong peaks found at 521 and 1074 cm^{-1}, representing Ni-O bond features of first (1P) and second-order (2P) phonon scattering, respectively [39,40], are substantially stronger compared to that of the Ni-S doublet. Figure 3b reveals the optical absorption property of the sample, in which the nickel oxysulfide exhibits a broad absorption peak started from ~350 nm with an extended edge to near-infrared spectrum. The Tauc plot is derived from the value of $(\alpha hv)^2$ against the optical energy (hv), indicating an indirect bandgap of ~1.43 eV for nickel oxysulfide [41]. Such a value is ~0.15 eV wider compared to that of the

original pure nickel sulfide (Figure S5), possibly due to the elevated temperature during the calcination treatment. The slight bandgap expansion is commonly seen in other metal oxysulfide materials [3,20].

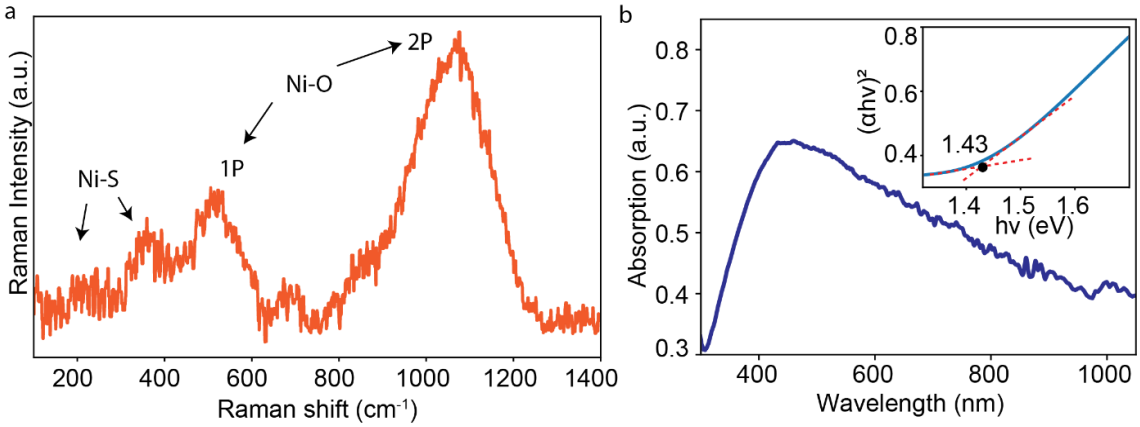

Figure 3. (**a**) Raman spectrum for nickel oxysulfide. (**b**) UV−Vis−NIR absorption spectrum and the corresponding Tauc plot shown in the inset.

3.2. Room Temperature Reversible Gas Sensor

To explore the gas sensing performance of the nickel oxysulfide micro-flowers, we prepared a transducing substrate possessing 200 pairs of interdigital electrodes (IDE) with a spacing of 10 µm. 20 µL of suspension containing 20 µg of material is drop-casted upon the substrate, forming a nickel sulfide sensor for gas sensing experiments. A customized gas chamber was used to contain the sensor, in which gas cylinders were connected to the inlet via a set of programmable mass flow controllers (MFCs). At the same time, the outlet was piped to a back pressure regulator to maintain a constant inner pressure of 1 standard atmosphere. The resistance of the sensor was continuously monitored by a multimeter through a minimized built-in probe stage inside the chamber during the experiment. The sensing response factor was calculated as the formula of $(R_{target} - R_{air})/R_{air} \times 100\%$, in which the R_{target} denotes the measuring resistance when the sensor is exposed to the target gas and the R_{air} represents the sensing resistance in the air [42–44]. We firstly investigated the room temperature gas response of the nickel oxysulfide sensor towards the H_2. As shown in Figure 4a and Figure S6, the nickel oxysulfide sensor demonstrated a fully recoverable dynamic response along with the increasing concentration of H_2 gas. Such a response was shown in an almost linear trend, eventually reaching a response factor of ~3.24% in 1% H_2. The corresponding response and recovery time, estimated as 90% and 10% of the full response magnitude, were ~20 min and ~33 min, respectively, according to Figure 4b. In addition, the repeatability of the sensor was tested in an 18 h continuous experiment as shown in Figure 4c. The sensor demonstrated an unnoticeable performance degradation after four cycles of tests of H_2 at a concentration of 1% with a repeatability error rate of 4.44%. Furthermore, the sensor was tested over a long period with an extraordinary long-term stability maintained after a constant experiment of five days (Figure S7). The sensor's reproducibility was confirmed on five unique samples in 1% H_2. From Figure S8, the sensors exhibited a highly consistent response to H_2 gas with an average response factor of ~3.07%. Finally, we confirmed the sensor's response to other commonly-seen gas species with industrial meaningful concentrations, including NO_2 (0.000126%), CH_4 (1%), and CO_2 (1%) under the same test conditions. As shown in Figure 4d and Figure S9, the corresponding response factors were found as ~0.027%, ~0.211%, and ~0.297%, respectively, which are at least one order less than that of 1% of H_2, revealing a high degree of selectivity [45]. Additionally, the nickel oxysulfide sensor was also assessed in a 60% relative humidity (RH) environment in comparison with dry background. According to Figure S10, the humidity showed minor impact to the sensor on the H_2 sensing performance. The calibration curves for selectivity gases are shown in Figure S11.

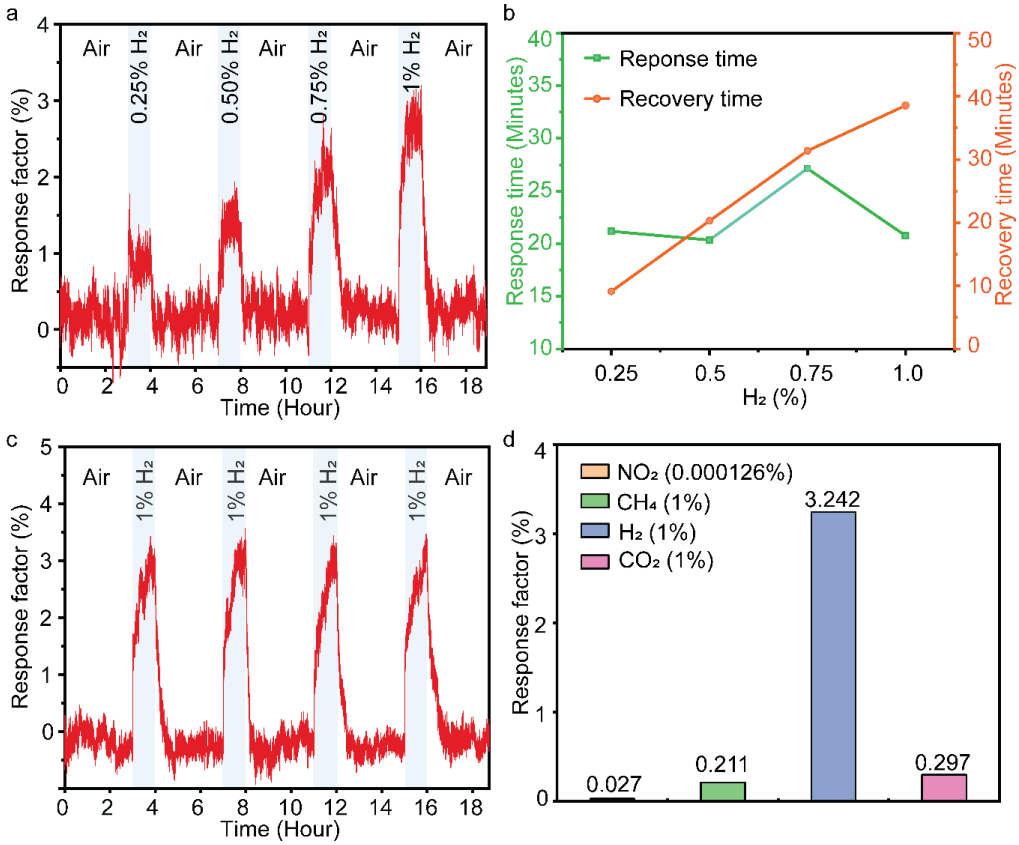

Figure 4. Gas sensing response for nickel oxysulfide at room temperature in the balance of air, (**a**) dynamic response toward H_2, (**b**) the corresponding response/recovery time. (**c**) repeatability and (**d**) selectivity.

Such a sensing performance was achieved at room temperature without any form of catalysts and external stimulus (e.g., light, heat, and bias voltage) involved, indicating that the sensing mechanism of nickel oxysulfide may be originating from the material surface interactions directly with physisorbed H_2 gas molecules [1,3,6,7,20]. The conventional chemosorption-based sensors rely on the catalytic interactions of chemisorbed oxygen ions with target gas molecules (usually oxidizing gases such as NO_2) in the presence of excitonic energy [46–48]. It is rarely seen a room temperature chemisorption-driven H_2 sensor with a fully reversible nature in the absence of the incorporation of metal catalysts [46–48]. On the other hand, some semiconductors with rich surface defects or well-designed nanostructures can demonstrate a fast response and full recovery phase at room temperature owing to their abundant oxygen vacancies [2,46]. However, they often show problems with selectivity and repeatability [46,49–52]. Given that, we believe that the sensing mechanism of the nickel oxysulfide sensor is dominated by physisorption rather than chemisorption. When hydrogen gas engages to the nickel oxysulfide surface, electrical dipoles are formed in the interface between the physisorbed H_2 molecules and the material interface, causing free charge carriers (i.e., holes) to be transferred from the material body to the H_2 molecules. Consequently, the electrical resistance of the nickel oxysulfide varied with the available holes in the material body, indicating a quantity change of the H_2 concentration inside the gas chamber.

4. Conclusions

We successfully obtained 3D nickel oxysulfide micro-flowers self-assembled from ultra-thin 2D nanoflakes through the calcination of nickel sulfide in a controlled environment. Through morphological analysis, the micro-flowers, with the major sizes between 5 and 10 μm, were composed of ultra-thin spherical nanoflakes with lateral dimensions of ~50 nm.

According to the structural and chemical composition analysis, most of the S atoms in the Ni-S framework were replaced by O atoms, leading to the crystal phase transition from initially hexagonal to orthorhombic coordination. Similar to other metal oxysulfides, the bandgap energy of nickel oxysulfide was slightly expanded to ~1.43 eV, which was ~0.15 eV wider compared to that of pure nickel sulfide. To evaluate the gas sensing performances, the change of electrical resistance of nickel oxysulfide was investigated upon the exposure of H_2 gas at room temperature without the application of external stimuli including light excitation and voltage biasing. A response factor of ~3.24% was found for 1% H_2 gas with an almost linear trend for the concentrations between 0.25% and 1%. In addition, a high degree of repeatability and full reversibility were demonstrated. Furthermore, the response magnitude of 1% H_2 was at least one order larger than several commonly seen gases including NO_2 (0.000126%), CH_4 (1%), and CO_2 (1%), revealing the excellent selectivity of H_2 which was rarely seen in pure semiconducting gas sensors. We considered that the physisorption mechanism governed the gas adsorption behavior over the surface of the ultra-thin nickel oxysulfide to enable the fully-reversible, highly selective, and room-temperature H_2 gas sensing performances, similar to the observation in the gas interaction with many types of 2D transition and post-transition metal sulfides. This work demonstrates the great potential of transition metal oxysulfides in high-performance physisorption-based gas sensing, which can be suitable candidates in developing low-cost and power-saving devices for the Internet of Things (IoT) applications.

Supplementary Materials: The following supporting information can be downloaded at: https://www.mdpi.com/article/10.3390/chemosensors10090372/s1, Figure S1: SEM image of the overall nickel oxysulfide sensor; Figure S2: SEM image for nickel sulfide particles upon a SiO_2 substrate; Figure S3: Theoretical crystal structure model of nickel oxysulfide ($NiSO_4$); Figure S4: EDS measurement of the nickel sulfide particles upon a SiO_2 substrate; Figure S5: UV-Vis-NIR absorption spectra of NiS with the corresponding Tauc-plot shown in the inset); Figure S6: Nickel oxysulfide dynamic response in H_2 (Resistance shown); Figure S7: Nickel oxysulfide long-term stability results at 1% H_2 over 5 days; Figure S8: Reproducibility results at 1% H_2 in air where nickel oxysulfide is deposited on 5 unique sensor substrates; Figure S9: Nickel oxysulfide selectivity response to 1% H_2, 0.000126% NO_2, 1% CH_4, 1% and 1% CO_2; Figure S10: The response curve of nickel oxysulfide in 1% H_2 in dry air and 60% RH; Figure S11: Nickel oxysulfide gas calibration curves for H_2, CO_2, CH_4 and NO_2.

Author Contributions: Conceptualization, J.Z.O., K.X., Z.L., G.R. and N.H.; data curation, K.X. and N.H.; formal analysis, K.X. and N.H.; funding acquisition, J.Z.O.; investigation, N.H., Y.C., R.O., Q.M., Y.H., V.T., H.Y., L.Z., X.L. and J.Z.; methodology, K.X. and N.H.; supervision, J.Z.O., G.R. and K.X.; validation, K.X., Z.L., G.R., N.H., Y.C., R.O., Q.M., Y.H., V.T., H.Y., L.Z., X.L. and J.Z.; visualization, K.X. and N.H.; writing—original draft, N.H.; writing—review and editing, J.Z.O., K.X. and G.R. All authors have read and agreed to the published version of the manuscript.

Funding: This work is supported by the National Natural Science Foundation of China (52172155), the scientific and technological projects for Distinguished Young Scholars of Sichuan Province (2020JDJQ0028), and the Fundamental Research Funds for the Central Universities (Grant No. 2682021CX107 and 2682021CX118).

Institutional Review Board Statement: Not applicable.

Informed Consent Statement: Not applicable.

Data Availability Statement: Not applicable.

Acknowledgments: N.H. would like to acknowledge The Australian Government Research Training Program (RTP) and RMIT University, School of Engineering (SoE) for the financial support. N.H would like to acknowledge the support of Food Agility CRC Ltd., funded under the Commonwealth Government CRC Program. The CRC program supports industry-led collaboration between industry, researchers, and the community. The authors would like to acknowledge the facilities, and the scientific and technical assistance of the RMIT Micro Nano Research Facility (MNRF) and the RMIT Microscopy & Microanalysis Facility (RMMF).

Conflicts of Interest: The authors declare no conflict of interest.

References

1. Ou, J.Z.; Ge, W.; Carey, B.; Daeneke, T.; Rotbart, A.; Shan, W.; Wang, Y.; Fu, Z.; Chrimes, A.F.; Wlodarski, W.; et al. Physisorption-Based Charge Transfer in Two-Dimensional SnS_2 for Selective and Reversible NO_2 Gas Sensing. *ACS Nano* **2015**, *9*, 10313–10323. [CrossRef]
2. Chung, M.G.; Kim, D.H.; Lee, H.M.; Kim, T.; Choi, J.H.; Seo, D.K.; Yoo, J.-B.; Hong, S.-H.; Kang, T.J.; Kim, Y.H. Highly sensitive NO_2 gas sensor based on ozone treated graphene. *Sens. Actuators B Chem.* **2012**, *166–167*, 172–176. [CrossRef]
3. Xu, K.; Zhang, B.Y.; Mohiuddin, M.; Ha, N.; Wen, X.; Zhou, C.; Li, Y.; Ren, G.; Zhang, H.; Zavabeti, A.; et al. Free-standing ultra-thin Janus indium oxysulfide for ultrasensitive visible-light-driven optoelectronic chemical sensing. *Nano Today* **2021**, *37*, 101096. [CrossRef]
4. Cho, B.; Yoon, J.; Lim, S.K.; Kim, A.R.; Kim, D.-H.; Park, S.-G.; Kwon, J.-D.; Lee, Y.-J.; Lee, K.-H.; Lee, B.H. Chemical sensing of 2D graphene/MoS_2 heterostructure device. *ACS Appl. Mater. Interfaces* **2015**, *7*, 16775–16780. [CrossRef] [PubMed]
5. Jannat, A.; Haque, F.; Xu, K.; Zhou, C.; Zhang, B.Y.; Syed, N.; Mohiuddin, M.; Messalea, K.A.; Li, X.; Gras, S.L.; et al. Exciton-Driven Chemical Sensors Based on Excitation-Dependent Photoluminescent Two-Dimensional SnS. *ACS Appl. Mater. Interfaces* **2019**, *11*, 42462–42468. [CrossRef] [PubMed]
6. Alkathiri, T.; Xu, K.; Zhang, B.Y.; Khan, M.W.; Jannat, A.; Syed, N.; Almutairi, A.F.M.; Ha, N.; Alsaif, M.M.Y.A.; Pillai, N.; et al. 2D Palladium sulphate for visible-light-driven optoelectronic reversible gas sensing at room temperature. *Small Sci.* **2021**, *2*, 2100097. [CrossRef]
7. Xu, K.; Ha, N.; Hu, Y.; Ma, Q.; Chen, W.; Wen, X.; Ou, R.; Trinh, V.; McConville, C.F.; Zhang, B.Y.; et al. A room temperature all-optical sensor based on two-dimensional SnS_2 for highly sensitive and reversible NO_2 sensing. *J. Hazard. Mater.* **2021**, *426*, 127813. [CrossRef]
8. Zhou, C.; Yang, W.; Zhu, H. Mechanism of charge transfer and its impacts on Fermi-level pinning for gas molecules adsorbed on monolayer WS_2. *J. Chem. Phys.* **2015**, *142*, 214704. [CrossRef]
9. Cheng, Y.; Li, Z.; Tang, T.; Xu, K.; Yu, H.; Tao, X.; Hung, C.M.; Hoa, N.D.; Fang, Y.; Ren, B.; et al. 3D micro-combs self-assembled from 2D N-doped In_2S_3 for room-temperature reversible NO_2 gas sensing. *Appl. Mater. Today* **2022**, *26*, 101355. [CrossRef]
10. Long, H.; Harley-Trochimczyk, A.; Pham, T.; Tang, Z.; Shi, T.; Zettl, A.; Carraro, C.; Worsley, M.A.; Maboudian, R. High Surface Area MoS_2/Graphene Hybrid Aerogel for Ultrasensitive NO_2 Detection. *Adv. Funct. Mater.* **2016**, *26*, 5158–5165. [CrossRef]
11. Mao, S.; Cui, S.; Lu, G.; Yu, K.; Wen, Z.; Chen, J. Tuning gas-sensing properties of reduced graphene oxide using tin oxide nanocrystals. *J. Mater. Chem.* **2012**, *22*, 11009–11013. [CrossRef]
12. Deng, S.; Tjoa, V.; Fan, H.M.; Tan, H.R.; Sayle, D.C.; Olivo, M.; Mhaisalkar, S.; Wei, J.; Sow, C.H. Reduced Graphene Oxide Conjugated Cu2O Nanowire Mesocrystals for High-Performance NO_2 Gas Sensor. *J. Am. Chem. Soc.* **2012**, *134*, 4905–4917. [CrossRef] [PubMed]
13. Huang, Y.; Jiao, W.; Chu, Z.; Wang, S.; Chen, L.; Nie, X.; Wang, R.; He, X. High Sensitivity, Humidity-Independent, Flexible NO_2 and NH_3 Gas Sensors Based on SnS_2 Hybrid Functional Graphene Ink. *ACS Appl. Mater. Interfaces* **2020**, *12*, 997–1004. [CrossRef] [PubMed]
14. Kang, I.-S.; So, H.-M.; Bang, G.-S.; Kwak, J.-H.; Lee, J.-O.; Ahn, C.W. Recovery improvement of graphene-based gas sensors functionalized with nanoscale heterojunctions. *Appl. Phys. Lett.* **2012**, *101*, 123504. [CrossRef]
15. Gautam, M.; Jayatissa, A.H. Ammonia gas sensing behavior of graphene surface decorated with gold nanoparticles. *Solid State Electron.* **2012**, *78*, 159–165. [CrossRef]
16. Sun, Q.; Wang, J.; Hao, J.; Zheng, S.; Wan, P.; Wang, T.; Fang, H.; Wang, Y. SnS_2/SnS p–n heterojunctions with an accumulation layer for ultrasensitive room-temperature NO_2 detection. *Nanoscale* **2019**, *11*, 13741–13749. [CrossRef] [PubMed]
17. Chen, H.; Chen, Y.; Zhang, H.; Zhang, D.W.; Zhou, P.; Huang, J. Suspended SnS_2 Layers by Light Assistance for Ultrasensitive Ammonia Detection at Room Temperature. *Adv. Funct. Mater.* **2018**, *28*, 1801035. [CrossRef]
18. Manh Hung, N.; Nguyen, C.V.; Arepalli, V.K.; Kim, J.; Duc Chinh, N.; Nguyen, T.D.; Seo, D.-B.; Kim, E.-T.; Kim, C.; Kim, D. Defect-Induced Gas-Sensing Properties of a Flexible SnS Sensor under UV Illumination at Room Temperature. *Sensors* **2020**, *20*, 5701. [CrossRef]
19. Gu, D.; Wang, X.; Liu, W.; Li, X.; Lin, S.; Wang, J.; Rumyantseva, M.N.; Gaskov, A.M.; Akbar, S.A. Visible-light activated room temperature NO_2 sensing of SnS_2 nanosheets based chemiresistive sensors. *Sens. Actuators B Chem.* **2020**, *305*, 127455. [CrossRef]
20. Zhou, H.; Xu, K.; Ha, N.; Cheng, Y.; Ou, R.; Ma, Q.; Hu, Y.; Trinh, V.; Ren, G.; Li, Z.; et al. Reversible Room Temperature H_2 Gas Sensing Based on Self-Assembled Cobalt Oxysulfide. *Sensors* **2022**, *22*, 303. [CrossRef]
21. Koo, W.-T.; Cho, H.-J.; Kim, D.-H.; Kim, Y.H.; Shin, H.; Penner, R.M.; Kim, I.-D. Chemiresistive Hydrogen Sensors: Fundamentals, Recent Advances, and Challenges. *ACS Nano* **2020**, *14*, 14284–14322. [CrossRef] [PubMed]
22. Stankova, M.; Vilanova, X.; Llobet, E.; Calderer, J.; Bittencourt, C.; Pireaux, J.J.; Correig, X. Influence of the annealing and operating temperatures on the gas-sensing properties of rf sputtered WO_3 thin-film sensors. *Sens. Actuators B Chem.* **2005**, *105*, 271–277. [CrossRef]
23. Khatibani, A.B. Investigation of gas sensing property of zinc oxide thin films deposited by Sol-Gel method: Effects of molarity and annealing temperature. *Indian J. Phys.* **2021**, *95*, 243–252. [CrossRef]
24. Yamazoe, N.; Shimanoe, K. Receptor Function and Response of Semiconductor Gas Sensor. *J. Sens.* **2009**, *2009*, 875704. [CrossRef]
25. Lee, S.P. Electrodes for Semiconductor Gas Sensors. *Sensors* **2017**, *17*, 683. [CrossRef]

26. Shombe, G.B.; Khan, M.D.; Zequine, C.; Zhao, C.; Gupta, R.K.; Revaprasadu, N. Direct solvent free synthesis of bare α-NiS, β-NiS and α-β-NiS composite as excellent electrocatalysts: Effect of self-capping on supercapacitance and overall water splitting activity. *Sci. Rep.* **2020**, *10*, 3260. [CrossRef]
27. Luo, P.; Zhang, H.; Liu, L.; Zhang, Y.; Deng, J.; Xu, C.; Hu, N.; Wang, Y. Targeted synthesis of unique nickel sulfide (NiS, NiS_2) microarchitectures and the applications for the enhanced water splitting system. *ACS Appl. Mater. Interfaces* **2017**, *9*, 2500–2508. [CrossRef]
28. Roffey, A.; Hollingsworth, N.; Islam, H.-U.; Mercy, M.; Sankar, G.; Catlow, C.R.A.; Hogarth, G.; de Leeuw, N.H. Phase control during the synthesis of nickel sulfide nanoparticles from dithiocarbamate precursors. *Nanoscale* **2016**, *8*, 11067–11075. [CrossRef]
29. Grosvenor, A.P.; Biesinger, M.C.; Smart, R.S.C.; McIntyre, N.S. New interpretations of XPS spectra of nickel metal and oxides. *Surf. Sci.* **2006**, *600*, 1771–1779. [CrossRef]
30. Zhang, L.; Huang, Y.; Zhang, Y.; Gu, H.; Fan, W.; Liu, T. Flexible Electrospun Carbon Nanofiber@NiS Core/Sheath Hybrid Membranes as Binder-Free Anodes for Highly Reversible Lithium Storage. *Adv. Mater. Interfaces* **2016**, *3*, 1500467. [CrossRef]
31. Jo, M.S.; Ghosh, S.; Jeong, S.M.; Kang, Y.C.; Cho, J.S. Coral-Like Yolk–Shell-Structured Nickel Oxide/Carbon Composite Microspheres for High-Performance Li-Ion Storage Anodes. *Nano-Micro Lett.* **2019**, *11*, 3. [CrossRef] [PubMed]
32. George, G.; Anandhan, S. Synthesis and characterisation of nickel oxide nanofibre webs with alcohol sensing characteristics. *RSC Adv.* **2014**, *4*, 62009–62020. [CrossRef]
33. Gu, Y.; Liu, S.; Li, C.; Cui, Q. Selective conversion of glycerol to acrolein over supported nickel sulfate catalysts. *J. Catal.* **2013**, *301*, 93–102. [CrossRef]
34. Gao, Y.; Wang, K.; Lin, Z.; Song, H.; Duan, X.; Peng, Z.; Yan, S. Hydrothermal Synthesis of Polyhedral Nickel Sulfide by Dual Sulfur Source for Highly-Efficient Hydrogen Evolution Catalysis. *Nanomaterials* **2020**, *10*, 2115. [CrossRef] [PubMed]
35. Bai, Z.; Li, S.; Fu, J.; Zhang, Q.; Chang, F.; Yang, L.; Lu, J.; Chen, Z. Metal-organic framework-derived Nickel Cobalt oxysulfide nanocages as trifunctional electrocatalysts for high efficiency power to hydrogen. *Nano Energy* **2019**, *58*, 680–686. [CrossRef]
36. Zhang, J.; Wang, Y.; Zhang, C.; Gao, H.; Lv, L.; Han, L.; Zhang, Z. Self-Supported Porous $NiSe_2$ Nanowrinkles as Efficient Bifunctional Electrocatalysts for Overall Water Splitting. *ACS Sustain. Chem. Eng.* **2018**, *6*, 2231–2239. [CrossRef]
37. Bishop, D.W.; Thomas, P.S.; Ray, A.S. Raman spectra of nickel(II) sulfide. *Mater. Res. Bull.* **1998**, *33*, 1303–1306. [CrossRef]
38. Cheng, Z.; Abernathy, H.; Liu, M. Raman Spectroscopy of Nickel Sulfide Ni_3S_2. *J. Phys. Chem.* **2007**, *111*, 17997–18000. [CrossRef]
39. Qiu, Z.; He, D.; Wang, Y.; Zhao, X.; Zhao, W.; Wu, H. High performance asymmetric supercapacitors with ultrahigh energy density based on hierarchical carbon nanotubes@NiO core–shell nanosheets and defect-introduced graphene sheets with hole structure. *RSC Adv.* **2017**, *7*, 7843–7856. [CrossRef]
40. Wang, H.; Yi, H.; Chen, X.; Wang, X. Asymmetric supercapacitors based on nano-architectured nickel oxide/graphene foam and hierarchical porous nitrogen-doped carbon nanotubes with ultrahigh-rate performance. *J. Mater. Chem. A* **2014**, *2*, 3223–3230. [CrossRef]
41. Makuła, P.; Pacia, M.; Macyk, W. How To Correctly Determine the Band Gap Energy of Modified Semiconductor Photocatalysts Based on UV–Vis Spectra. *J. Phys. Chem. Lett.* **2018**, *9*, 6814–6817. [CrossRef] [PubMed]
42. Quan, W.; Hu, X.; Min, X.; Qiu, J.; Tian, R.; Ji, P.; Qin, W.; Wang, H.; Pan, T.; Cheng, S.; et al. A Highly Sensitive and Selective ppb-Level Acetone Sensor Based on a Pt-Doped 3D Porous SnO_2 Hierarchical Structure. *Sensors* **2020**, *20*, 1150. [CrossRef]
43. Lin, T.; Lv, X.; Hu, Z.; Xu, A.; Feng, C. Semiconductor Metal Oxides as Chemoresistive Sensors for Detecting Volatile Organic Compounds. *Sensors* **2019**, *19*, 233. [CrossRef] [PubMed]
44. Wang, Z.; Zhi, M.; Xu, M.; Guo, C.; Man, Z.; Zhang, Z.; Li, Q.; Lv, Y.; Zhao, W.; Yan, J.; et al. Ultrasensitive NO_2 gas sensor based on Sb-doped SnO_2 covered ZnO nano-heterojunction. *J. Mater. Sci.* **2021**, *56*, 7348–7356. [CrossRef]
45. Morrison, S.R. Selectivity in semiconductor gas sensors. *Sens. Actuators A* **1987**, *12*, 425–440. [CrossRef]
46. Cheng, Y.; Ren, B.; Xu, K.; Jeerapan, I.; Chen, H.; Li, Z.; Ou, J.Z. Recent progress in intrinsic and stimulated room-temperature gas sensors enabled by low-dimensional materials. *J. Mater. Chem. C.* **2021**, *9*, 3026–3051. [CrossRef]
47. Li, M.; Hu, M.; Jia, D.; Ma, S.; Yan, W. NO_2-sensing properties based on the nanocomposite of n-WO3−x/n-porous silicon at room temperature. *Sens. Actuators B Chem.* **2013**, *186*, 140–147. [CrossRef]
48. Ji, H.; Zeng, W.; Li, Y. Gas sensing mechanisms of metal oxide semiconductors: A focus review. *Nanoscale* **2019**, *11*, 22664–22684. [CrossRef]
49. Krivetsky, V.; Ponzoni, A.; Comini, E.; Rumyantseva, M.; Gaskov, A. Selective modified SnO_2-based materials for gas sensors arrays. *Procedia Chem.* **2009**, *1*, 204–207. [CrossRef]
50. Fort, A.; Serrano-Santos, M.B.; Spinicci, R.; Ulivieri, N.; Vignoli, V. Electronic noses based on metal oxide gas sensors: The problem of selectivity enhancement. In Proceedings of the Proceedings of the 21st IEEE Instrumentation and Measurement Technology Conference (IEEE Cat. No.04CH37510), Como, Italy, 18–20 May 2004; Volume 591, pp. 599–604.
51. Xu, L.-H.; Wu, T.-M. Synthesis of highly sensitive ammonia gas sensor of polyaniline/graphene nanoribbon/indium oxide composite at room temperature. *J. Mater. Sci. Mater. Electron.* **2020**, *31*, 7276–7283. [CrossRef]
52. Dennler, N.; Rastogi, S.; Fonollosa, J.; van Schaik, A.; Schmuker, M. Drift in a popular metal oxide sensor dataset reveals limitations for gas classification benchmarks. *Sens. Actuators B Chem.* **2022**, *361*, 131668. [CrossRef]